Available online at www.sciencedirect.com

SciVerse ScienceDirect

Journal of the European Ceramic Society 32 (2012) 2529–2536

www.elsevier.com/locate/jeurceramsoc

Spark-plasma sintering of ZrB_2 ultra-high-temperature ceramics at lower temperature via nanoscale crystal refinement

Victor Zamora [a], Angel L. Ortiz [a,*], Fernando Guiberteau [a], Mats Nygren [b]

[a] *Departamento de Ingeniería Mecánica, Energética y de los Materiales, Universidad de Extremadura, Badajoz, Spain*
[b] *Department of Materials and Environmental Chemistry, University of Stockholm, 10691 Stockholm, Sweden*

Received 30 November 2011; received in revised form 12 February 2012; accepted 16 February 2012
Available online 13 March 2012

Abstract

We have explored the feasibility of reducing the spark-plasma-sintering (SPS) temperature of additive-free ZrB_2 ultra-high-temperature ceramics (UHTCs) via crystal size refinement of the starting powder down to the low nanoscale. We found that under otherwise the same SPS conditions (75 MPa pressure, and 100 °C/min heating ramp) nanoscale ZrB_2 can be densified at temperatures about 450 °C lower than for the typical micrometre and submicrometre ZrB_2 powders, and at least 250 °C below the ultra-fine powder temperature. Furthermore, the nanoscale crystal refinement also promotes the production of fine-grained ZrB_2 UHTCs. We also found that elimination of the B_2O_3 impurities plays an important role in the complete densification. The unequalled sinterability of the nanoscale ZrB_2 powders highlights the need to use high-energy ball-milling for the comminution of the typical commercially available ZrB_2 powders.

Keywords: ZrB_2; Ultra-high-temperature ceramics; Sintering; High-energy ball-milling

1. Introduction

Zirconium diboride (ZrB_2) is one of the few compounds that can be classed as ultra-high-temperature ceramics (UHTC).[1] Its favourable set of properties (among others, melting point 3250 °C, hardness 23 GPa, elastic modulus >500 GPa, electrical resistivity $\sim 10^{-5}\ \Omega$ cm, and thermal conductivity >60 W m^{-1} K^{-1}) makes ZrB_2 a very attractive candidate material in the world of extreme environment engineering for such applications as hypersonic flight, scramjet and rocket propulsion, atmospheric re-entry, refractory crucibles, and plasma-arc electrodes, to cite just some.[2,3]

It is widely recognized by the ceramics community that one of the greatest obstacles to the successful development and implementation of ZrB_2 UHTCs is their poor sinterability, to which various intrinsic and extrinsic factors contribute. The former include the strong covalent bonding, the low self-diffusion coefficients, and the large particle sizes that together impose severe kinetic restrictions on the diffusion,[2–5] and among the latter is contamination by surface oxides that favours coarsening over densification.[2,3,5] The strategy typically adopted to tackle the problem of ZrB_2's poor sinterability is to introduce sintering additives (either liquid phase formers, or reactive agents) together with the refinement of the starting powders by ball milling (normally in the form of wet attrition milling) down to the submicrometre scale.[2,3] Regarding this latter point, in a recent study we investigated in detail the spark-plasma sintering (SPS) kinetics of ZrB_2 without additives as a function of the crystal size from a couple of micrometres down to a few nanometres (achieved by high-energy ball-milling), and concluded that the breakthrough needed to obtain ZrB_2 powders with unmatched sintering behaviour requires going beyond the simple refinement to the submicrometre scale, and that it is nanoscale crystal refinement which offers an unprecedented opportunity to significantly reduce the sintering temperature of ZrB_2.[6] This latter expectation, which until now has not been confirmed experimentally, arises from the observation that only nanoscale crystal refinement promotes considerably greater grain-boundary diffusion at much lower temperatures in ZrB_2,[6] and this is the mass transport mechanism responsible for the material's densification. Elucidating this pending issue of the role of the crystal refinement

* Corresponding author. Tel.: +34 924289600x86726; fax: +34 924289601.
E-mail addresses: alortiz@materiales.unex.es, alortiz@unex.es (A.L. Ortiz).

0955-2219/$ – see front matter © 2012 Elsevier Ltd. All rights reserved.
doi:10.1016/j.jeurceramsoc.2012.02.023

scale in reducing the sintering temperature of ZrB_2 is thus a fundamental question requiring a prompt experimental response not only because lower-temperature sintering is one of the long sought for objectives in the field of UHTCs, but also because, if confirmed, it could have important implications regarding the comminution practices employed by the UHTC community.

With this in mind, the objective of the present work is to extend the previous kinetics study by conducting the first extensive set of SPS experimental measurements explicitly designed to explore by means of a detailed densification study the question of the crystal refinement scale in reducing the sintering temperature of ZrB_2. For this proof-of-concept study, we spark-plasma sintered six ZrB_2 powders with varied crystal sizes in the micrometre, submicrometre, and nanometre scales, without the introduction of sintering additives to thus investigate crystal-size effects without this interference. The details of the experiments and the major findings are described below.

2. Experimental procedure

The six ZrB_2 powders used in the present study were taken from the broader set of ZrB_2 powders utilized in the previous SPS kinetics study.[6] We shall thus here only summarize their preparation protocol. Briefly, the coarse powder with an average crystal size of 2 μm was obtained from a commercial source (Grade B, H.C. Starck, Germany). The powders with submicrometre and ultra-fine crystals (∼500 and 160 nm, respectively), and the three powders with nanometre crystals (∼70, 25, and 10 nm) were prepared by subjecting the commercial ZrB_2 powder to high-energy ball-milling in air in a shaker mill (Spex D8000, Spex CertiPrep, USA) for different times as required to reach the desired average crystal size,[6] using WC balls as milling media with a ball-to-powder weight ratio of 4:1. More details of the preparation and characteristics of these ZrB_2 powders can be found elsewhere.[6–9] However, it is also important to mention here that to prevent the powder contamination during high-energy ball-milling, a first milling cycle was carried out with the objective of depositing a thin film of ZrB_2 on the surface of the container and of the balls, and the resulting powder was thrown away. Then, the milling cycle was repeated utilizing the same container and balls, using the resulting powder for this study. With this milling procedure, (i) WC contamination was only detected in the powder ball-milled for 180 min, but not in the rest of powders, and in a minimal amount of ∼0.9 vol% according to the Rietveld analysis of the X-ray diffraction (XRD) pattern collected with a high-resolution diffractometer, and (ii) no Fe contamination was detected in any of the ball-milled powders.[9] The direct measurement carried out here through the weight loss of the balls indicates however that the contamination by WC is indeed lower than 0.5 vol%. This WC contamination degree is about 4–6 times lower than that introduced typically with other common milling procedures, which is due to the combination of many factors such as the two-milling protocol adopted here, the low charge ratio (i.e., the ball-to-powder weight ratio) of 4 used in this study, and the more than likely differences in other milling parameters (for example size, density, and surface roughness of the WC balls, wettability of the ZrB_2 powder towards the WC balls at the milling condition, extent of filling of the container, and milling atmosphere and environment, to name a few), as well as to the fact that the shaker mills operate with compressive forces whereas the attritors and the conventional mills function with a combination of shear and compressive forces.

The different ZrB_2 powders were individually loaded into 12-mm diameter graphite dies lined with graphite foil and surrounded by a 1 cm thick graphite blanket to minimize heat loss, and were then spark-plasma sintered (Dr. Sinter SPS-2050, Sumitomo Coal Mining Co., Japan) in a dynamic vacuum atmosphere (i.e., 6 Pa). The graphite die has a wall thickness of 9 mm, and has a hole machined in its central region of 2.5 mm depth. Two types of SPS cycles were implemented: (i) heating at 100 °C/min up to the target temperature under 75 MPa pressure, and soaking at these conditions of temperature and pressure for a certain time (henceforth termed the simple SPS cycle), and (ii) heating at 100 °C/min up to the target temperature under 20 MPa pressure, followed by soaking at the target temperature under 75 MPa pressure for a certain time (henceforth termed the complex SPS cycle). Details of another SPS cycle used only sporadically will be given along with the corresponding results. For each ZrB_2 powder, the target temperature (measured by an optical pyrometer focused on the interior of hole of the graphite die[c]) was considered as a variable, setting its values in accordance with the reference of its transition temperature from surface diffusion to grain-boundary diffusion (T_{GBD}) determined in the previous kinetics study[6] (i.e., ∼1550, 1650, 1740, 1765, 1785, and 1810 °C for the crystal sizes of 10, 25, 70, 160, 500, and 2000 nm, respectively). After the completion of the SPS cycle, the load was released and the electrical power was shut off to allow rapid cooling (in 1–2 min) to room temperature. The SPS furnace is equipped with a dilatometer of resolution better than 0.001 mm, connected to a computer to log the shrinkage curves. These curves were corrected for the expansion of the graphite parts (i.e., die, punches, and spacers) to give the real shrinkage curves of the powders themselves, and were then converted to densification curves by considering the relative densities of the sintered samples. The sintered materials were examined by scanning electron microscopy (FE-SEM; S4800-II, Hitachi, Japan) to validate the porosity data, and also to observe their microstructure. The SEM observations were done on fracture surfaces, at 5 kV without metal coating.

3. Results and discussion

The T_{GBD} data obtained in the previous SPS kinetics study[6] suggested that the ZrB_2 nano-powder with 10-nm crystals would exhibit the lowest sintering temperature of all the powders to be

[c] It is a well-known fact in SPS that the actual temperature inside the specimen is greater than the temperature measured by the optical pyrometer. However, a previous SPS study on HfB_2 and HfC [10], which have both thermal and electrical conductivities similar to ZrB_2, has shown that for the same graphite die and experimental configuration than used here the temperature mismatch is in the range 100–125 °C at 1700 °C and around 250 °C at 2200 °C. With this information, the temperature mismatch up to 1625 °C is estimated to be not greater than 50–75 °C.

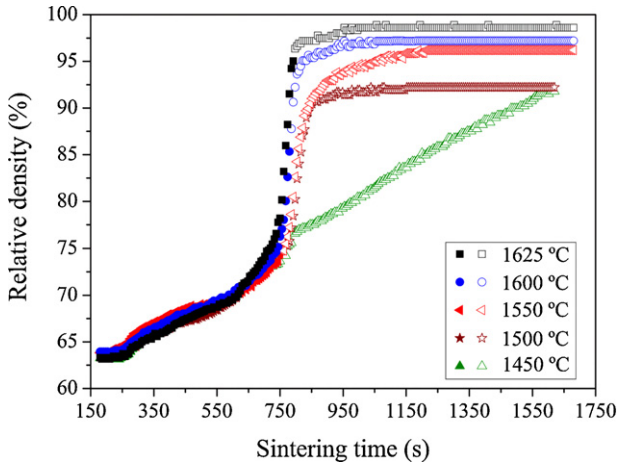

Fig. 1. Densification curves as a function of time for the ZrB_2 nano-powder with 10-nm crystals, obtained with the simple SPS cycle for target temperatures of 1450, 1500, 1550, 1600, and 1625 °C. Solid symbols correspond to data measured during the heating ramp up to the target temperature, and open symbols to data measured during the soaking.

investigated here, for which reason the first set of SPS densification experiments were focused on this powder. Fig. 1 compares the densification curves as a function of time for this ZrB_2 nano-powder, obtained with the simple SPS cycle after 15 min of soaking at 1450, 1500, 1550, 1600, and 1625 °C. It is clear that the final degree of densification increases with increasing target temperature, from ~91% at 1450 °C to ~98.5% at 1625 °C. The latter can be considered to be a dense UHTC. Since the densification curve at 1625 °C stabilized after 3.5 min of isothermal soaking, there is no reason to prolong further the sintering as this would only cause coarsening. One notes that the target temperature of 1625 °C is fairly close to the corresponding value of T_{GBD} (~1550 °C), with only ~75 °C difference. Hence, these results confirm the possibility of densifying ZrB_2 UHTCs close to the temperature dictated by T_{GBD} under appropriate isothermal soaking. This notion is further supported by the observation in Fig. 1 that the final degree of densification is relatively moderate (less than 93%) after 15 min of isothermal heating at 1450 and 1500 °C, which both are temperatures below the value of T_{GBD}, but that it increases to greater than 96% when the sintering is performed for the same duration time at 1550 °C or at higher temperatures. This trend was also evident in the direct examination of the microstructures by SEM, as illustrated by way of example in the comparison of micrographs in Fig. 2 which shows incomplete densification at 1450 °C but pore absence at 1625 °C. In principle, it could be argued that this near-complete densification at a temperature as low as 1625 °C is assisted by the 0.5 vol% WC contamination through the oxide removal reaction $ZrO_2 + 3WC \rightarrow ZrC + 3W + 2CO(g)$[11] since thermodynamic calculations indicate that this reaction is favourable above ~1260 °C under the vacuum of 6 Pa. To explore this possibility, because for example the reaction could not be kinetically favourable, the sample sintered at 1625 °C has been analysed by XRD. If the XRD pattern shows the presence of the reaction products ZrC and W, it could then be concluded that WC plays a role; otherwise, there

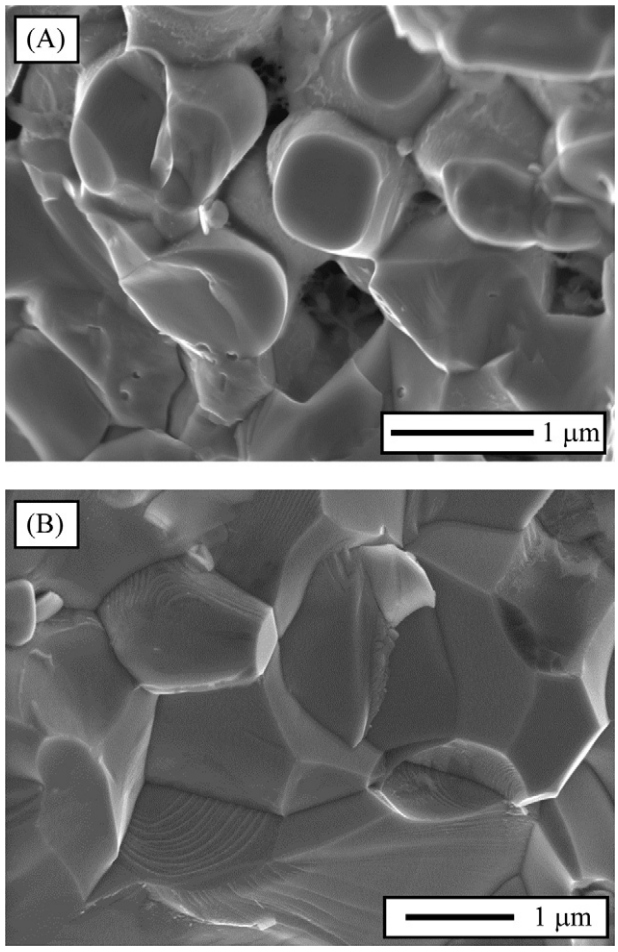

Fig. 2. SEM micrographs of the UHTCs fabricated from the ZrB_2 nano-powder with 10-nm crystals using the simple SPS cycle for 15 min at (A) 1450 °C and (B) 1625 °C.

is no role played by WC. The XRD pattern of the sample sintered at 1625 °C in Fig. 3 shows, beside the ZrB_2 peaks, the presence of ZrO_2 and WC peaks (i.e., of the reactants) but not of ZrC or W peaks (i.e., of the reaction products). Other reduction reactions of ZrO_2 by WC would also lead to the formation of ZrC, which is not observed here. Thus, this XRD analysis reveals the absence of role played by WC during the present SPS treatment, and, consequently, indicates that the near-complete densification observed at 1625 °C must be attributed to the crystal size refinement of the starting powder down to the low nanoscale.

Another interesting observation in Fig. 1 is that all the densification curves reached the plateau after several minutes of isothermal soaking, except the curve obtained at 1450 °C which has still not flattened out after 15 min. In this last case, it appeared that the ZrB_2 nano-powder would have densified further with a more prolonged soaking at 1450 °C. Consequently, we measured the densification curve of the ZrB_2 nano-powder at 1450 °C until the stabilization of the graphite punches. The result is shown in Fig. 4. This measurement indicates that ~98% relative density can be reached with the simple SPS cycle after 30 min at 1450 °C. Interestingly, this is almost the same final degree of densification reached at 1625 °C (~98.5%), and is slightly greater than those reached at 1550 (~96%) and 1600 °C

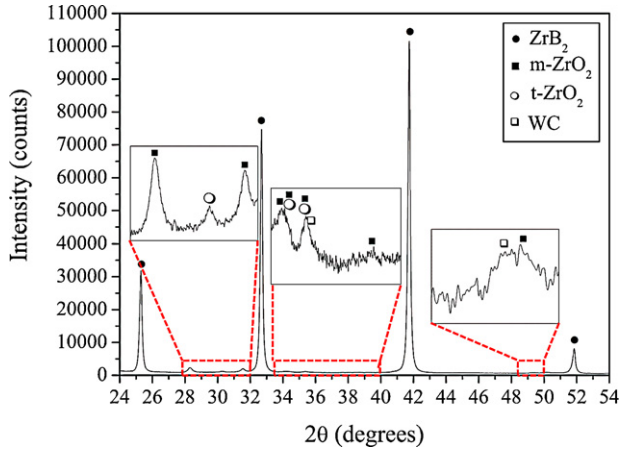

Fig. 3. X-ray diffraction pattern of the UHTC fabricated from the ZrB_2 nano-powder with 10-nm crystals using the simple SPS cycle at 1625 °C for 15 min. The phase identification is included. The insets show magnificated regions in logarithmic Y-scale to facilitate the appreciation of the weak ZrO_2 and WC peaks. The XRD data were collected in step-scanning mode with monochromatic Cu-Kα_1 radiation (λ = 1.54183 Å), using a high-resolution laboratory diffractometer (D8 Advance, Bruker AXS, Germany).

(∼97%) and much greater than that at 1500 °C (∼92%), in all cases after the corresponding curve stabilization. This was an unexpected finding because it is not what we would have predicted considering simply that the diffusion coefficients obey an Arrhenius-type law.[12] Therefore, to shed light on this question, we examined by SEM the sample fabricated at 1450 °C. As one observes in the micrograph of Fig. 5, the detailed SEM observations revealed that some grain faces exhibit what appears to have been a liquid phase. We believe that this liquid is boria, and that it is responsible for the unexpected anomalously high densification at 1450 °C because the presence of liquid boria facilitates not only grain sliding but also mass transport. This boria forms because the high-energy ball-milling was done in air, so that ZrB_2 can oxidize superficially during the milling, and also because the resulting ZrB_2 nano-powder passivates

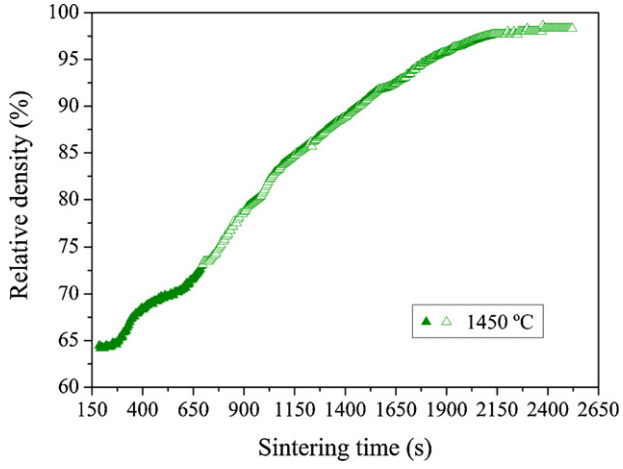

Fig. 4. Densification curve as a function of time for the ZrB_2 nano-powder with 10-nm crystals, obtained with the simple SPS cycle for a target temperature of 1450 °C. The closed symbols correspond to data measured during the heating ramp up to 1450 °C, and the open symbols to data measured during the soaking at 1450 °C.

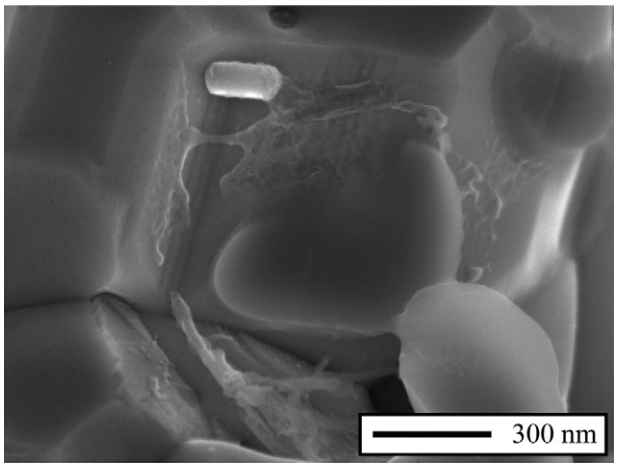

Fig. 5. High-magnification SEM micrograph of the UHTC fabricated from the ZrB_2 nano-powder with 10-nm crystals using the simple SPS cycle at 1450 °C for 30 min.

spontaneously in contact with air.[13] The evolution of the vacuum level during the SPS test at 1450 °C supports the presence of liquid boria deduced from the SEM observations. Thus, the vacuum level hardly changed throughout the experiment (almost constant at ∼6 Pa), indicating that no detectable boria gas emission occurred at 1450 °C and therefore that boria remained in the liquid state. This scenario was, however, totally different during the SPS experiments at higher temperatures in which gas release was indeed detected, with the vacuum level temporarily dropping a couple of Pa or more and then recovering its initial level. Given this information, it is reasonable to conclude that, despite the SPS at 1450 °C eventually resulting in near-complete densification, this low-temperature densification is not useful because the residual boria will make the resulting ZrB_2 material degrade in service when exposed to ultra-high-temperature applications. Thus, 1625 °C continues to be the best SPS temperature.

Since the objective pursued is the lower-temperature SPS of boria-free ZrB_2 UHTCs, the following step was to focus on the possible optimization of the SPS cycle between 1450 and 1625 °C. The SEM observations such as that shown in Fig. 6 for the UHTC processed at 1500 °C indicated that the residual pores in the UHTCs fabricated with the simple SPS cycle have a near-perfect spherical shape, thus suggesting that they originated from the slow outward diffusion of the boria gas occluded when the pore distribution transformed very rapidly from open porosity to closed porosity in the presence of pressure.[d] In consequence, one possible manner of facilitating the escape of the boria gas generated would be to apply a lower compaction pressure during the heating ramp in order to delay the collapse of the open pore structure so that the gasses can leave the

[d] According to solid-state sintering theory, the transformation from open porosity to closed porosity occurs during the intermediate stage of sintering, which covers normally the interval of relative densities between 70 and 90% [14]. Thus, 90% densification represents typically the onset of the final stage of sintering, which is the sintering regime where the closed porosity is eliminated [14]. Consequently, within the confines of the present study, 90% relative density will henceforth be taken to be the moment of the collapse of the open pore structure.

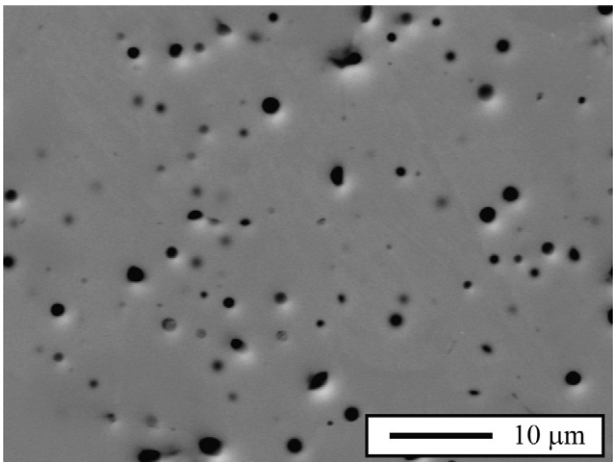

Fig. 6. Low-magnification SEM micrograph of the UHTC fabricated from the ZrB_2 nano-powder with 10-nm crystals using the simple SPS cycle at 1500 °C for 15 min.

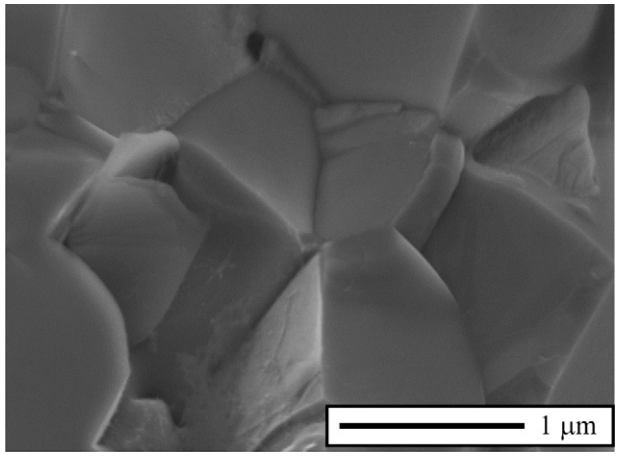

Fig. 8. SEM micrograph of the UHTC fabricated from the ZrB_2 nano-powder with 10-nm crystals with the complex SPS cycle at 1625 °C for 15 min.

sample more easily. To explore this possibility, we performed new experiments using the complex SPS cycle described in Section 2. Fig. 7 shows the resulting densification curves as a function of time for the ZrB_2 nano-powder obtained with the complex SPS cycle after 15 min of soaking at 1500, 1550, 1600, and 1625 °C. Recall that the temperature of 1450 °C had been excluded from further analysis due to the undesired presence of residual boria in the microstructure. As can be observed in Fig. 7, these curves exhibit the same trend as was seen before in Fig. 1, with the final degree of densification increasing with increasing target temperature. The comparison between the densification curves obtained with the simple and complex SPS cycles is very interesting however. One can infer that in all cases the densification was better during the first moments (i.e., approximately the first 750 s) with the simple SPS cycle doubtless due to the greater compaction pressure (75 vs 20 MPa), but that the ultimate densification was essentially the same with both cycles (i.e., ∼92.5% at 1500 °C, 96% at 1550 °C, 97% at 1600 °C, and

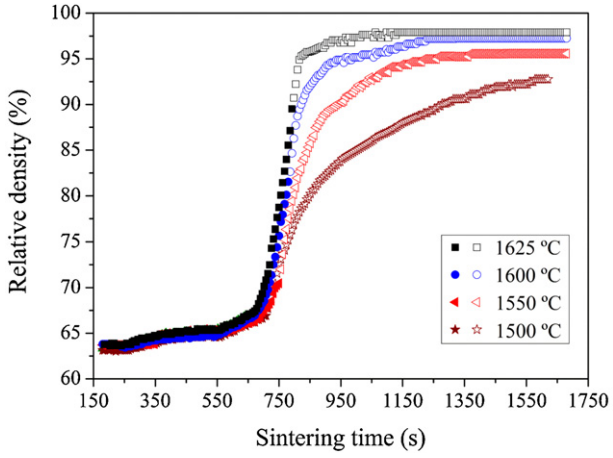

Fig. 7. Densification curves as a function of time for the ZrB_2 nano-powder with 10-nm crystals, obtained with the complex SPS cycle for target temperatures of 1500, 1550, 1600, and 1625 °C. The closed symbols correspond to data measured during the heating ramp up to the target temperature, and the open symbols to data measured during the soaking.

98% at 1625 °C). One can thus conclude that the complex SPS cycle by itself is not effective in improving the final degree of densification. Neither does the complex SPS cycle seem to affect appreciably the grain size, as deduced by comparing for example the SEM micrograph in Fig. 8 for the sample fabricated with the complex cycle at 1625 °C with the corresponding micrograph in Fig. 2B for the simple SPS cycle. These observations indicate that the microstructure (i.e., porosity and grain size) is dictated essentially by the high-pressure/high-temperature stretch. Nevertheless, comparison of the curves of Figs. 1 and 7 merits further attention. Clearly, one sees that, except for the above-mentioned differences during the first moments of SPS, the shapes of the densification curves at 1550, 1600, and 1625 °C are otherwise very similar for the two SPS cycles, and that at these temperatures the use of the complex SPS cycle does little to delay the end of the collapse of the open pore structure (i.e., by ∼90, 30 and 20 s, respectively). Consistent with this scenario, we measured at 1550, 1600, and 1625 °C only a marginal difference between the evolution of the vacuum levels during the simple and complex SPS cycles. The 1500 °C densification curves exhibit, however, a relevant variation in shape since, with the complex SPS cycle, the approach to the limiting value of ∼92.5% is far more gradual. Indeed, the open pore structure collapses much later (i.e., ∼500 s later). Interestingly, we now indeed noted at 1500 °C a relevant difference in the boria emission. In particular, with the complex SPS cycle not only was the gas emission peak 2 Pa more intense and longer lasting than with the simple SPS cycle, but at 1500 °C the same level was reached as at 1625 °C with the simple SPS cycle despite the temperature being 125 °C lower. Unfortunately, despite the better elimination of boria gas at 1500 °C with the complex SPS cycle, the final densification degree reached was still only moderate due to the insufficient diffusion at that temperature.

Considering all these analyses together, we decided to test a two-step SPS cycle with a first step at 1500 °C for ∼10 min under a moderate pressure of 20 MPa to eliminate the boria impurities while densifying the compact up to ∼90% relative density with little coarsening, followed by a shorter second step at 1600 °C under a higher pressure of 75 MPa to promote the complete pore

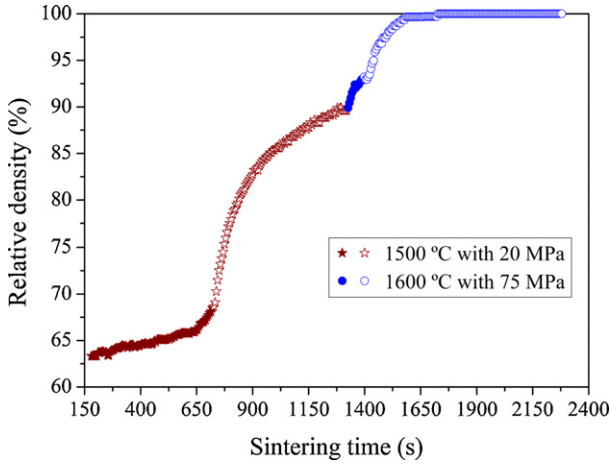

Fig. 9. Densification curves as a function of time for the ZrB_2 nano-powder with 10-nm crystals, obtained with the two-step SPS cycle comprising a first simple SPS cycle under 20 MPa pressure with a target temperature of 1500 °C, followed by a second complex SPS cycle with a target temperature of 1600 °C. The closed symbols correspond to data measured during the heating ramp up to the target temperatures, and the open symbols to data measured during the corresponding soakings.

elimination. These expectations were indeed borne out experimentally because, as shown in the densification curve of Fig. 9 and in the SEM micrograph of Fig. 10, a fully dense ZrB_2 compact was obtainable with this two-step SPS cycle. Note that, although this present proposal of a two-step cycle and the one typically used to process nano-ceramics pursue the same objective of densification with little grain boundary migration, their procedures are reversed with respect to each other.[15] In the latter, the powder is first heated at the high temperature for a short period, and then rapidly cooled to a lower temperature and maintained there for a long period. In the present case the main concern is to eliminate the boria impurities, which requires a "smooth" intermediate stage of sintering, while in the typical nano-ceramics processing case the principal concern is inhibition of grain growth, which requires a "smooth" final stage of sintering.

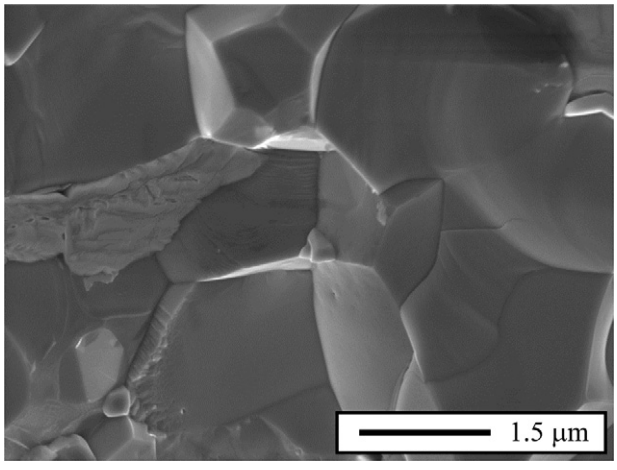

Fig. 10. SEM micrograph of the UHTC fabricated from the ZrB_2 nano-powder with 10-nm crystals with the two-step SPS cycle at 1600 °C for 15 min.

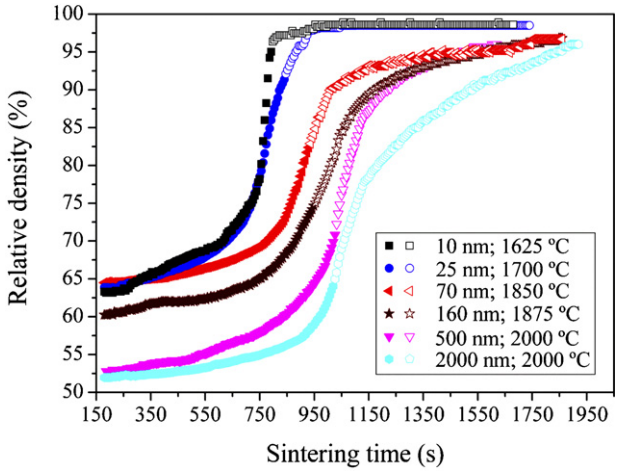

Fig. 11. Densification curves as a function of time for the ZrB_2 coarse, submicrometre, ultra-fine, and nanometre powders, obtained with the simple SPS cycle at the lowest target temperatures that resulted in final densification degrees greater than 95%. The closed symbols correspond to data measured during the heating ramp up to the corresponding target temperature, and the open symbols to data measured during the soaking. The fact that the degree of densification at the onset of the SPS cycle first increases and then decreases is simply because the powder's mechanical-packing density scales inversely with the particle sizes, not with the crystal sizes, and the nano-crystals achieved with the long-time high-energy ball-milling are actually agglomerated.[6,8,9]

To put the ZrB_2 nano-powder with 10-nm crystals results into perspective, in the following we shall compare the above SPS data with those of ZrB_2 powders with larger crystal sizes of ~25, 70, 160, 500, and 2000 nm. Given that the experimental observations indicated that the simple and complex SPS cycles yielded eventually the same degree of densification and similar microstructure, the SPS experiments for these ZrB_2 powders with larger crystal sizes were conducted using only the simple SPS cycle which was clearly sufficient for the purposes of the present comparative study. Fig. 11 is a comparison of the lowest-temperature densification curves for all these ZrB_2 powders, with the lowest temperature being that which satisfied the condition of reaching at least 95% densification. Note that the measurements of the data comprising these curves required many SPS experiments to be carried out at different temperatures for each of these ZrB_2 powders in the same way as was done previously for the nano-powder with 10-nm crystals, although, for the sake of brevity, these densification curves will not be presented. As one observes, the curves in Fig. 11 demonstrate clearly that the crystal size refinement progressively reduces the SPS temperature of ZrB_2, and also that the reduction is only moderate with the refinement to the ultra-fine range, but very marked with the refinement to the low nanoscale. Indeed, since according to Fig. 1 the ZrB_2 nano-powder with 10-nm crystals reached 96% densification at 1550 °C, which is the densification reached by the micrometre and submicrometre powders at 2000 °C (see Fig. 11), one can thus conclude that the nanoscale crystal refinement reduced the SPS temperature by not less than 450 °C for the typical crystal sizes of the most-widely used ZrB_2 powders. This reduction is very relevant because it is similar to or even greater than the temperature reductions previously achieved with the aid of former liquid-phase

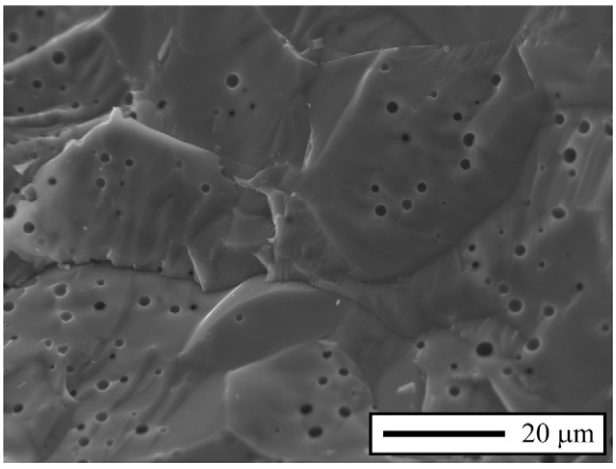

Fig. 12. SEM micrograph of the UHTC fabricated from the submicrometre ZrB_2 powder with 0.5 μm crystals with the simple SPS cycle at 2000 °C for 15 min.

sintering additives (for example with $MoSi_2$ or with $TaSi_2$).[2,3] In addition, there was no attempt here to prevent oxygen contamination (which is known to promote coarsening[2,3,5,16,17]) by use of an inert atmosphere during the milling, suggesting that there could be still room for further reductions in the sintering temperature, but at the expense of making the comminution routine more tedious and costly. Another additional benefit of the nanoscale crystal refinement is that it allows fine-grained microstructures to be obtained (see Figs. 2B, 8, and 10) instead of the coarse-grained microstructures resulting from the sintering of the typical micrometre or submicrometre starting powders (Fig. 12), an aspect that is very important to provide the ZrB_2 UHTCs with superior strength.[2,3]

Finally, the present study has interesting implications for comminution practices in the UHTC community. In particular, it emerges that the preparation of ZrB_2 powders with unequalled sintering behaviour necessarily requires the use of high-energy ball-milling because the typical wet attrition milling, which has so far been the gold-standard comminution treatment, is a form of conventional milling that does not generate the high compressive stresses in the ball-to-ball collisions needed to refine the crystal sizes down to nanoscale. This, however, does not rule out attritor use because this technique can also function as a high-energy ball-mill if operated in dry with a high ball-to-powder ratio (>40:1) and with a high peripheral speed of the agitator (>3 m/s). This would be another way of achieving the nanoscale crystal refinement needed to make the lower-temperature sintering of ZrB_2 possible.

4. Conclusions

We have investigated the effect of the crystal refinement scale on the lower-temperature densification of ZrB_2 UHTCs by SPS without additives. The results allow the following conclusions to be drawn:

1. The lower-temperature limit for the SPS densification of ZrB_2 decreases continuously with decreasing crystal size in the starting powder.
2. Under otherwise identical SPS conditions (i.e., 75 MPa pressure, and 100 °C/min heating ramp), nanoscale ZrB_2 has been densified at 1625 °C, well below the 2000 °C required for the typical micrometre and submicrometre powders to reach only 96% densification and the corresponding 1875 °C for the ultra-fine powder. Thus, crystal size refinement to the low nanoscale constitutes one of the long hoped-for breakthrough solutions to the fundamental problem of the poor sinterability of ZrB_2.
3. Nanoscale ZrB_2 can be densified at temperatures as low as 1450 °C favoured by the presence of B_2O_3 liquid phase, but this low-temperature sintering with non-transient B_2O_3 is not useful for ultra-high-temperature applications.
4. The complete densification of ZrB_2 UHTCs requires the use of sintering cycles that promote the total elimination, via evaporation, of the B_2O_3 impurities. This is especially relevant in the case of SPS because the rapid collapse of the open pore structure facilitates the trapping of the B_2O_3 gas generated within the closed pores.
5. Nanoscale crystal refinement promotes the production of fine-grained microstructures, derived from the combination of the smaller crystal sizes in the starting powders and the lower sintering temperatures required for densification.
6. High-energy ball-milling can provide ZrB_2 with the superior sinterability which is not otherwise achievable today by the standard comminution method of wet attrition milling.

Acknowledgements

This work was supported by the Ministerio de Ciencia y Tecnología (Government of Spain) and FEDER funds under Grant No. MAT 2007-61609.

References

1. Wuchina E, Opila E, Opeka M, Fahrenholtz W, Talmy I. UHTCs: ultra-high temperature ceramic materials for extreme environment applications. *Interface* 2007;**16**(4):30–6.
2. Fahrenholtz WG, Hilmas GE, Talmy IG, Zaykoski JA. Refractory diborides of zirconium and hafnium. *J Am Ceram Soc* 2007;**90**(5):1347–64.
3. Guo S-Q. Densification of ZrB_2-based composites and their mechanical and physical properties: a review. *J Eur Ceram Soc* 2009;**29**(6): 995–1011.
4. Telle R, Sigl LS, Takagi K. Boride-based hard materials. In: Riedel R, editor. *Handbook of ceramic hard materials*, vol. 2. Weinheim: Wiley-VCH; 2000. pp. 802–945.
5. Thompson M, Fahrenholtz WG, Hilmas G. Effect of starting particle size and oxygen content on densification of ZrB_2. *J Am Ceram Soc* 2011;**94**(2):429–35.
6. Zamora V, Ortiz AL, Guiberteau F, Nygren M. Crystal-size dependence of the spark-plasma-sintering kinetics of ZrB_2 ultra-high-temperature ceramics. *J Eur Ceram Soc* 2012;**32**(2):271–6.
7. Galán CA, Ortiz AL, Guiberteau F, Shaw LL. Crystallite size refinement of ZrB_2 by high-energy ball milling. *J Am Ceram Soc* 2009;**92**(12): 3114–7.

8. Galán CA, Ortiz AL, Guiberteau F, Shaw LL. High-energy ball milling of ZrB_2 in the presence of graphite. *J Am Ceram Soc* 2010;**93**(10): 3072–5.
9. Zamora V, Ortiz AL, Guiberteau F, Shaw LL, Nygren M. On the crystallite size refinement of ZrB_2 by high-energy ball-milling in the presence of SiC. *J Eur Ceram Soc* 2011;**31**(13):2407–14.
10. Sciti D, Guicciardi S, Nygren M. Densification and mechanical behavior of HfC and HfB_2 fabricated by spark plasma sintering. *J Am Ceram Soc* 2008;**91**(5):1433–40.
11. Fahrenholtz WG, Hilmas GE, Zhang SC, Zhu S. Pressureless sintering of zirconium diboride: particle size and additive effects. *J Am Ceram Soc* 2008;**91**(5):1398–404.
12. Mehrer H. *Diffusion in solid metals and alloys*. Springer-Verlag; 1990.
13. Ortiz AL, Zamora V, Rodríguez-Rojas F. A study of the oxidation of ZrB_2 powders during high-energy ball-milling in air. *Ceram Int* 2012;**38**(4):2857–63.
14. German RM. *Sintering theory and practice*. Wiley: New York; 1996.
15. Chen I-W, Wang X-H. Sintering dense nano-crystalline ceramics without final stage grain growth. *Nature* 2000;**404**(6774): 168–71.
16. Chamberlain AL, Fahrenholtz WG, Hilmas GE. Pressureless sintering of zirconium diboride. *J Am Ceram Soc* 2006;**89**(2): 450–6.
17. Zhang SC, Hilmas GE, Fahrenholtz WG. Pressureless densification of zirconium diboride with boron carbide additions. *J Am Ceram Soc* 2006;**89**(5):1544–50.